International Journal for Housing Science and Its Applications
Publish August 4, 2025. Volume 46, Issue 3 Pages 1587-1599

https://doi.org/10.70517/ijhsa463122

Comprehensive assessment study of optical storage charging microgrid output on distribution network stability based on computational analysis

Qingsheng Li[1,*], Jian Wang[1], Yu Zhang[1], Zhaofeng Zhang[1], Zhen Li[1] and Zhanpeng Xu[2]
[1] Power Grid Planning Research Center, Guizhou Power Grid Co., Ltd., Guiyang, Guizhou, 550002, China
[2] China Energy Engineering Corporation Guangdong Electric Power Design Institute Co., Ltd., Guangzhou, Guangdong, 510663, China
Corresponding authors: (e-mail: 17728117081@163.com).

Abstract With the increase of renewable energy penetration, the power fluctuation of optical storage charging microgrids poses a serious challenge to the stability of distribution networks. In this paper, a comprehensive assessment framework based on computational analysis is proposed to quantify the static and dynamic impacts of new energy outputs on the distribution network by constructing a multi-microgrid system topology model and a wind-optical-hydrogen cooperative regulation mechanism. The system-level and device-level constraint models are established by combining the connectivity graph theory, covering the branch voltage balance, node power limit, and the dynamic boundaries of the state of charge (SOC) of energy storage. A combined direct-indirect prediction method is designed to realize short-term and long-term prediction for the strong stochasticity of photovoltaic, wind turbine output and load power. The hydrogen production-storage-generation system is further introduced to smooth out new energy fluctuations by modeling hydrogen production and power regulation capability. Simulation experiments based on Matlab/Simulink show that the prediction accuracy of the proposed prediction model reaches 95.18% for photovoltaic output and 80.71% for wind turbine output. Under the optimized configuration strategy, the critical value of energy storage SOC is controlled at 89.45%, while the MPPT is 90.13%, which is more than 90% and is harmful to the safety of the energy storage device. The peak system load power is 606.41W, which is not exceeded. Comparing with KPCA, attention mechanism and other methods, the average assessment accuracy of voltage stability based on computational analysis is 99.18%, TSI=1.0, Gmean=99.48, which significantly improves the disturbance resistance of distribution network.

Index Terms computational analysis, optical storage and charging microgrid, distribution network stability, output prediction, grid connection characteristics

I. Introduction

With the gradual implementation of China's “carbon peak, carbon neutral” energy saving and emission reduction strategy, high penetration rate of new energy grid will become the basic feature of the power system and development pattern [1], [2]. Microgrids give full play to the advantages of local new energy for power generation, both lower cost, less pollution and more flexible and other characteristics, coupled with the microgrid anti-hazardous ability, and to ensure the security and stability of the power energy supply and other advantages, and has gradually become the focus of the world's power industry [3]-[6]. Microgrid is mainly composed of distributed power supply, energy storage equipment, conversion equipment, monitoring and protection equipment, and loads, which can be regarded as a small-scale power generation, distribution and consumption system [7]-[9]. It can effectively solve the problems of incorporating new and renewable energy sources into the grid system and digesting such energy sources on a large scale, which is a feasible technology path with high flexibility and orderliness [10]-[12].

In order to alleviate the problems of power supply, relevant enterprises at home and abroad have begun to introduce the photovoltaic storage charging microgrid technology. It can effectively improve the customer-side bus voltage stability, meet the requirements of the user's power quality, and also improve the utilization rate of photovoltaic power generation [13], [14]. The use of enterprise photovoltaic storage and charging microgrids can solve the power supply of enterprise loads during peak electricity consumption at low cost and short construction period [15]. It can also make part of the important loads of enterprises run stably when the distribution network is disconnected, realize the role of peak shaving and valley filling, and reduce the production cost of enterprises while also making profits through the peak and valley electricity price difference [16], [17]. And it can also charge new energy vehicles for industrial enterprises through charging pile facilities, which improves the consumption capacity of intermittent energy and the utilization rate of existing distribution grid resources [18], [19]. Therefore, optical

storage and charging microgrids are of great significance for improving the economic operation and power supply reliability of the power system, and promoting China's energy transition and economic and social development [20].

However, the intermittent and uncertain characteristics of the grid-connected output of new energy with high penetration rate pose new challenges to the flexible operation of the power system [21]. The integration of distributed generation systems into microgrids changes the microgrid structure from unidirectional to bidirectional currents, and its structure is also changed from a radioactive structure to a multi-power structure [22], [23]. The traditional current calculation, especially the magnitude and direction of short-circuit current, is not applicable to the case of distributed power microgrid, and similarly, the setting of relay protection and other actions should be reconsidered [24], [25]. Therefore, the introduction of a computational analysis model to assess the impact of the optical storage and charging microgrid on the power quality and power supply sufficiency of the distribution network will be conducive to the safe operation of the power system.

This study focuses on the core objective of comprehensively assessing the impact of optical storage-charged microgrid output on the stability of the distribution network, and proposes a full-chain methodological framework of systematic modeling, output prediction, and grid-connected characteristic analysis to provide theoretical support for quantitative assessment and optimal control. By constructing a multi-microgrid system topology model based on the connectivity graph theory, we propose system-level constraints (branch voltage balance, node power balance, etc.) and equipment-level constraints (power limits for photovoltaic, wind turbine, energy storage, etc.) to ensure that the model conforms to the actual operating conditions, and to clarify system-level and equipment-level constraints to lay a mathematical foundation for stability analysis. Secondly, for the intermittency and load uncertainty of renewable energy and the strong stochasticity of PV and wind, a forecasting strategy combining direct and indirect methods is proposed, and short-term and long-term load forecasts are distinguished to provide data support for dynamic scheduling of microgrids. Further, a wind-photovoltaic-hydrogen synergistic microgrid system structure is introduced to smooth out new energy fluctuations through the hydrogen production-storage-generation system, and a synergistic system comprising hydrogen production, storage and power generation is designed to quantify the hydrogen production and power regulation capability through mathematical modeling to mitigate the impact of new energy fluctuations on the power grid and enhance the resilience of the system. Based on the data acquisition and preprocessing technology, we also combine static analysis (voltage deviation, harmonic distortion) and dynamic analysis (ARIMA time series model) to evaluate the comprehensive impact of PV grid integration on the stability of the distribution network.

II. Optical storage and charging microgrid modeling, output prediction and grid-connected characterization methods

II. A.Modeling of the power grid component

In general, a multi-microgrid system model can be represented by a connectivity graph $M=(N,E)$. Where N denotes the set of all nodes with node numbers $i=1,2,....,i\in N$; E denotes the set of all branches, and there exists $(i,j)\in E$ denoting the branch from node i to node j. If the multi-microgrid system consists of G microgrids, these G microgrids correspond to nodes $i=1,2,...,G,i\in N$. The branch connection relationship between microgrids and microgrids in the multi-microgrid system can be represented by E. The set of nodes as well as the set of branch circuits within each microgrid can be regarded as another connectivity graph $m=(n,e)$, and the set of nodes as well as the set of branch circuits within each microgrid can be denoted by n as well as e, respectively. A (multi-)microgrid network topology consisting of 5 nodes and 4 branches is shown in Fig. 1.

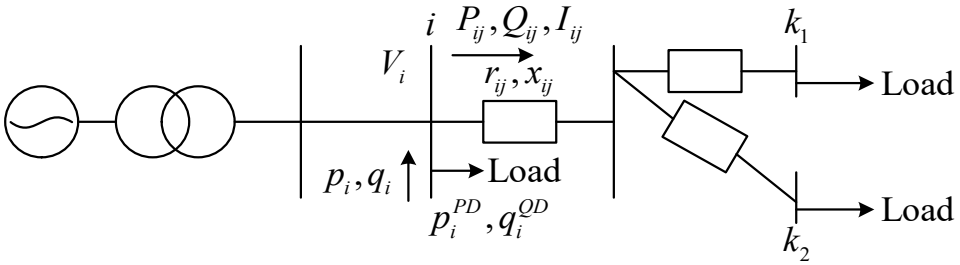

Figure 1: Microgrid network topology

In the figure, i,j,k_1,k_2 all denote the node numbers in the (multi-)microgrid; for any node $i,p_i,p_i^{P_D}$ denote the injected active power and the active load of the node, respectively, and v_i denotes the voltage magnitude of the node; for a branch (i,j), P_{ij} denotes the active power at the beginning of the branch, Q_{ij} denotes the reactive

power at the beginning of the branch, I_{ij} denotes the magnitude of the current flowing through the branch, r_{ij} denotes the resistance on the branch, and x_{ij} denotes the reactance on the branch.

II. A. 1) System-level constraints

The currents between microgrids have similar mathematical expressions as the currents within microgrids. In the trend model, it mainly contains branch voltage balance, node injected active power balance, node injected reactive power balance and branch power balance, which can be expressed as follows:

Branch circuit voltage balance:

$$V_j^2 = V_i^2 + (r_{ij}^2 + x_{ij}^2)I_{ij}^2 - 2(r_{ij}P_{ij} + x_{ij}Q_{ij}) \forall (i,j) \in E, i \in N, j \in W \tag{1}$$

The node injects the active power balance:

$$\sum_{(j,k)\in E} P_{jk} - \sum_{(i,j)\in E} (P_{ij} - r_{ij}I_{ij}^2) = p_j \forall i \in N, j \in W \tag{2}$$

Nodes inject reactive power balance:

$$\sum_{(j,k)\in E} Q_{jk} - \sum_{(i,j)\in E} (Q_{ij} - x_{ij}I_{ij}^2) = p_j \forall i \in N, j \in W \tag{3}$$

Branch circuit power balancing:

$$P_{ij}^2 + Q_{ij}^2 = I_{ij}^2 V_i^2 \quad \forall (i,j) \in E, i \in N \tag{4}$$

In order to meet the power quality standards and ensure reliable power supply, the node voltage must be maintained within the permissible range. The upper as well as lower limits of the node voltage are denoted as $v_{\min}$ and $v_{\max}$, respectively, and the value of the node voltage is limited to the upper and lower limits:

$$V_{\min} \le V_{i,t} \le V_{\max} \tag{5}$$

II. A. 2) Device-level constraints

To ensure system stability, nodes with generation capacity must have safe and reasonable active and reactive power ranges.

The active power range of solar PV panels is defined as follows:

$$0 \le P_{i,t}^{PV} \le P_{i\max}^{PV} \tag{6}$$

where $P_{i,t}^{PV}$ denotes the active power generated by node i PV panels at moment t; and $P_{i\max}^{PV}$ denotes the upper limit of active power generated by PV panels.

The wind turbine active power range is defined as follows:

$$0 \le P_{i,t}^{WT} \le P_{i\max}^{WT} \tag{7}$$

where $P_{i,t}^{WT}$ denotes the active power generated by the turbine at node i at moment t; and $P_{i\max}^{WT}$ denotes the upper limit of the active power generated by the turbine.

The active power range of the electric heat conversion unit is defined as follows:

$$0 \le P_{i,t}^{P2H} \le P_{i\max}^{P2H} \tag{8}$$

where $P_{i,t}^{P2H}$ denotes the active power of the node i electric heat conversion unit at the t moment; $P_{i\max}^{P2H}$ denotes the upper limit of the active power of the electric heat conversion unit.

The climbing constraint of the diesel generator is defined as follows:

$$P_{i,t}^{DEG} - P_{i,t-\Delta t}^{DEG} \le R_{up}^{DEG}\Delta t \cdot s_{t-\Delta t}^{DEG} + P_{i\min}^{DEG}(s_t^{DEG} - s_{t-\Delta t}^{DEG}) + P_{i\max}^{DEG}(1 - s_t^{DEG}) \tag{9}$$

$$P_{i,t-\Delta t}^{DEG} - P_{i,t}^{DEG} \le R_{dn}^{DEG}\Delta t \cdot s_t^{DEG} + P_{i\min}^{DEG}(s_{t-\Delta t}^{DEG} - s_t^{DEG}) + P_{i\max}^{DEG}(1 - s_{t-\Delta t}^{DEG}) \tag{10}$$

where $P_{i,t}^{DEG}$ represents the active power produced by the diesel generator located at node i at moment t; Restricted to a minimum power $P_{i\min}^{DEG}$ and a maximum power $P_{i\max}^{DEG}$ range $P_{i\min}^{DEG} \le P_{i,t}^{DEG} \le P_{i,\max}^{DEG}$;The Δt represents the moment gap; $P_{i,t-\Delta}^{DEG}$ represents the power generated by the diesel generator at the moment $t-\Delta t$; R_{up}^{DEG} and R_{dn}^{DEG} denote the diesel generator active up and down limits, respectively; and the binary variable s_i^{DEU} denotes whether or not the diesel generator is in the operating state (1 means it is in the operating state, and 0 means it is in the off state).

The upper and lower limits of the active energy storage system are defined as follows:

$$-P_{i\max}^{ESS} \le P_{i,t}^{ESS} \le P_{i\max}^{ESS} \tag{11}$$

where $P_{i,t}^{ESS}$ denotes the active power of the energy storage system located at node i at moment t; $P_{i\max}^{ESS}$ denotes the maximum active power of the energy storage system.

The upper and lower bounds of the state of charge (SOC) $SOC_{i,t}^{ESS}$ of the energy storage system located at node i at moment t are shown below:

$$SOC_{i\min}^{ESS} \le SOC_{i,t}^{ESS} \le SOC_{i\max}^{ESS} \tag{12}$$

where $SOC_{i\max}^{ESS}$ represents the upper limit of the battery charge state; $SOC_{i\min}^{ESS}$ represents the lower limit of the battery charge state.

The relationship between the reactive power $Q_{i,j}^{K}$ and active power $P_{i,j}^{K}$ and capacity of the inverters of the photovoltaic, wind turbine, diesel generator, and energy storage system is shown below:

$$(P_{i,t}^{PV})^2 + (Q_{i,t}^{PV})^2 \le (S_{i\max}^{PV})^2 \tag{13}$$

$$(P_{i,t}^{WT})^2 + (Q_{i,t}^{WT})^2 \le (S_{i\max}^{WT})^2 \tag{14}$$

$$(P_{i,j}^{DEG})^2 + (Q_{i,j}^{DEG})^2 \le (S_{i\max}^{DEG})^2 \tag{15}$$

$$(P_{i,t}^{ESS})^2 + (Q_{i,t}^{ESS})^2 \le (S_{i\max}^{ESS})^2 \tag{16}$$

where S_i^K denotes the capacity of the inverter connected to node i and $K = \{PV, WT, DEG, ESS\}$.

II. B.Output and load power prediction

After completing the modeling and constraints analysis of the multi-microgrid system, the strong uncertainty of renewable energy output and load power needs to be further addressed. This section focuses on the prediction methods for PV, wind power and load power, which provide key data inputs for real-time power dispatch and optimal control of microgrids through the combination of direct and indirect methods.

The PV power output is directly related to the intensity of sunshine, with strong intermittency, volatility and stochasticity, while PV power generation has a relatively high proportion in new energy microgrids, which has a significant impact on the quality of the power grid. Therefore, accurate prediction of photovoltaic power generation is of great significance for grid regulation and control and stable operation. There are 2 main methods for PV power prediction.

(1) Direct prediction, i.e., based on the cyclic characteristics of sunshine and meteorological information, the output power of PV system is directly predicted by the historical output power of PV system in the grid and previous meteorological information;

(2) Indirect prediction, i.e., power prediction is carried out based on the actual current local insolation and meteorological conditions, combined with the actual configuration of the PV system and the output model.

The power prediction of wind power generation system is similar to that of PV system, in which the direct method is mainly through the local climate and the historical data of wind power generation output, and directly predicts the power characteristics under the current time period, which has a lower prediction accuracy, but the method is simple and more efficient. Indirect method is mainly through the local topography, meteorological information, weather station data, etc. through the actual model for prediction, this method is highly accurate, but the model is complex and inefficient.

For a new energy microgrid in a particular scenario, its internal load type and power are relatively fixed, and the load power prediction is mainly divided into short-term prediction and long-term prediction. Short-term prediction focuses on the cyclic change characteristics of the load inside the microgrid, taking into account the power demand of different loads in different time periods, climate, operational demand and other conditions, and predicts the load power in advance to guide the regulation and control of the microgrid's internal output. Long-term forecasting is mainly based on the local development plan, climate characteristics and other factors, predicting the change of load demand, in order to guide the allocation of energy capacity of each new energy source within the grid, to ensure that it can meet the local long-term power demand.

II. C.Wind-Photo-Hydrogen Microgrid System Structure

Based on the accurate output and load prediction results, how to effectively smooth the impact of new energy fluctuations on the distribution network becomes critical. This section proposes a wind-light-hydrogen synergistic

microgrid system structure, which converts intermittent electric energy into hydrogen energy storage and feedback by constructing a dynamic equilibrium model of hydrogen production, storage and power generation, which significantly improves the flexibility and reliability of the system.

II. C. 1) Wind turbine output modeling

Fluctuations in wind speed are usually described by a two-parameter Weibull model:

$$F(V)=P(v\le V)=1-\exp\left[-\left(\frac{V}{b}\right)^{k}\right] \tag{17}$$

where v is the wind speed; h is the shape parameter; and b is the scale parameter.

The mathematical model of wind power output power is constructed as:

$$P_i(v_i)=\begin{cases}0 & v_i<v_{in},v_i>v_{cat}\\ \dfrac{v_i-v_{in}}{v_{rated}-v_{in}}\omega_i & v_{in}\le v_i\le v_{rated}\\ v_i & v_{rated}<v_i<v_{cat}\end{cases} \tag{18}$$

where v_{in},v_{cat} and v_{rated} are the cut-in wind speed, cut-out wind speed and rated wind speed, respectively; and ω_i is the total installed capacity of the WTGs.

II. C. 2) Modeling of PV Generator Outputs

The light intensity at a given time period is generally described by a Beta (Beta) distribution:

$$f(S)=\frac{\Gamma(\alpha+\beta)}{\Gamma(\alpha)\Gamma(\beta)}(\frac{S}{S_{\max}})^{w-1}(1-\frac{S}{S_{\max}})^{\beta-1} \tag{19}$$

where α and β are the 2 parameters of the Beta distribution: $\Gamma(\cdot)$ is the gamma function. The expression for the relationship between the light intensity S and the output power produced by the PV system is:

$$P_{PVG}=\begin{cases}P_{PVG,r}\dfrac{S}{S_t},S\le S_t\\ P_{PVG,r},S>S_t\end{cases} \tag{20}$$

where $P_{PVG,r}$ is the rated output power of the PVG; S_r is the rated light intensity.

II. C. 3) Hydrogen production - hydrogen storage - power generation systems

Introducing a system incorporating hydrogen production, storage and power generation as an energy regulation mechanism.

Mitigating erratic fluctuations in wind and photovoltaic output power.

$$W_{EC,i}=P_{EC,i}\eta_{EC}\omega \tag{21}$$

$$P_{PC,i}=\frac{W_{PC,i}}{\tau}\eta_{PC} \tag{22}$$

$$E_{HST,i+1}-E_{HST,i}=\eta_{HST}^{d,i}W_{HST,i}^{d,i}-\frac{W_{HST,i}^{d,i}}{\eta_{HST}^{d,i}} \tag{23}$$

where $W_{EC,i}$ and $W_{PC,i}$ are the amount of hydrogen produced and consumed, respectively; $P_{EC,i}$ and $P_{PC,i}$, are the power of electrolysis and the power of output, respectively; η_{EC} and η_{PC} are the efficiencies of EC and FC, respectively; ω and τ are the amount of hydrogen produced and consumed per unit of electrical energy electrolyzed, respectively; $E_{HST,t},E_{HST,t+1}$ are the amount of hydrogen stored in the HST at the moment of t and $t+1$, respectively; $W_{HST,i}^{chs},W_{HST,i}^{ds}$ are the hydrogen storage and release, respectively; $\eta_{HST}^{chs},\eta_{HST}^{dis}$ are the hydrogen storage and release efficiency, respectively.

II. D.Grid connection characterization

On the basis of optimizing the internal structure and energy regulation mechanism of microgrids, the actual impact of new energy grid integration on distribution networks needs to be further quantified. In this section, we systematically evaluate the voltage deviation, harmonic distortion and power fluctuation caused by PV grid integration from data acquisition, pre-processing to static and dynamic characterization to provide empirical evidence for the comprehensive assessment of distribution network stability.

II. D. 1) Data acquisition and pre-processing

Obtaining high-quality data is the basis of PV grid-connected characterization, which mainly comes from the operation monitoring equipment of distributed PV systems, including PV inverters, power conditioners, and monitoring nodes of the distribution grid. The collected data include PV output power, grid voltage, frequency, total harmonic distortion (THD), ambient temperature and solar radiation intensity. The data preprocessing process requires cleaning of the raw data to eliminate missing values, outliers and invalid data. Data cleaning methods include the use of statistical properties (e.g., mean and standard deviation) to detect outliers and interpolation algorithms to complete missing values. Data feature extraction is an important step in preprocessing analyzing the main feature variables according to the formula. For time series data $x(t)$, the harmonic components can be analyzed using Fast Fourier Transform (FFT) to calculate the total harmonic distortion rate e.g.:

$$THD-\sqrt{\sum_{a=2}^{\infty}(\frac{V_n}{V_1})^2}\times 100\% \tag{24}$$

Where V_n denotes the nth harmonic voltage and V_1 is the fundamental voltage. In addition, the fluctuation amplitude analysis can be used to express the stability of the power output using the standard deviation σ as in equation (25):

$$\sigma-\sqrt{\frac{1}{N}\sum_{i=1}^{N}(P_i-\mu)^2} \tag{25}$$

where P_i is the sampled value of PV output power, μ is the average power, and N is the total number of sampling points. These preprocessing and feature extraction processes provide high quality input data for subsequent analysis.

II. D. 2) Grid connection characterization

PV grid-connected characterization includes the evaluation of static and dynamic characteristics. Static characteristics focus on the impact of PV grid-connectedness on the grid, such as power quality problems, voltage deviation and frequency stability, while dynamic characteristics analyze the impact of PV output fluctuations on the transient response of the grid. Based on big data technology can statistically analyze historical data to construct a probability distribution model of grid-connected performance. The statistical distribution of voltage deviation ΔV can be expressed as equation (26).

$$P(\Delta V)=\frac{1}{\sqrt{2\pi\sigma^2}}\exp(-\frac{(\Delta V-\mu)^2}{2\sigma^2}) \tag{26}$$

where μ and σ are the mean and standard deviation of the voltage deviation, respectively. Dynamic characterization is usually combined with a time series model, such as the autoregressive integral sliding average (ARIMA) based modeling method. Let the time series of PV output power be X_t, and its model can be expressed as equation (27).

$$X_t=\phi_1X_{t-1}+\phi_2X_{t-2}+\cdots+\phi_pX_{t-p}+\theta_1\dot{o}_{t-1}+\theta_2\dot{o}_{t-2}+\cdots+\theta_q\dot{o}_{t-q}+\dot{o}_t \tag{27}$$

where ϕ is the autoregressive parameter, θ is the moving average parameter, and $\dot{o}_t$ is the white noise. By estimating the model parameters, it is possible to predict the short-term variation of PV output power and analyze its potential impact on grid stability. In addition to this environmental factors have a significant impact on the grid connection characteristics. For example, the solar radiation intensity I and ambient temperature T directly determine the PV output power P, and the relationship can be expressed as equation (28).

$$P=P_{STC}\cdot\frac{I}{I_{STC}}\cdot[1+\alpha(T-T_{STC})] \tag{28}$$

where P_{STC} is the rated power under standard test conditions, I_{STC} and T_{STC} are the standard irradiation intensity and temperature, respectively, and α is the temperature coefficient. Combined with big data analysis, the long-term impact of environmental changes on the grid-connected performance can be evaluated to support the optimization of control strategies.

III. Simulation experiment verification

After completing the theoretical design of multi-microgrid system modeling, output prediction method and wind-optical-hydrogen synergistic structure, in order to verify the feasibility of the proposed model and the effectiveness of the control strategy, this chapter builds a simulation platform based on Matlab/Simulink, and carries out a systematic experimental analysis from the dimensions of the energy storage operation safety, output prediction accuracy, optimal configuration strategy and voltage stability assessment, etc., to provide empirical support to comprehensively assess the impact of optical storage and charging microgrid on the stability of the distribution network.

III. A. Safety of energy storage operations

In order to maximize the lifetime of the energy storage device and ensure its safe operation, the prevention of overcharging and discharging is crucial. The control strategy proposed in this paper adopts a dynamic approach to adjust the operating constraints based on the state SOC of the energy storage device. In order to verify the safety of the control strategy proposed in this study under the critical state of SOC, a series of simulation tests under extreme conditions are conducted in this paper. Setting the ambient temperature T=25°C constant, the light intensity I=1000W/m² is analyzed as an example, and the following figure shows the simulation when the SOC is at the charging critical value. Fig. 2 demonstrates the frequency variation, Fig. 3 shows the variation of PV output power and energy storage output power, and Fig. 4 shows the variation of energy storage SOC.

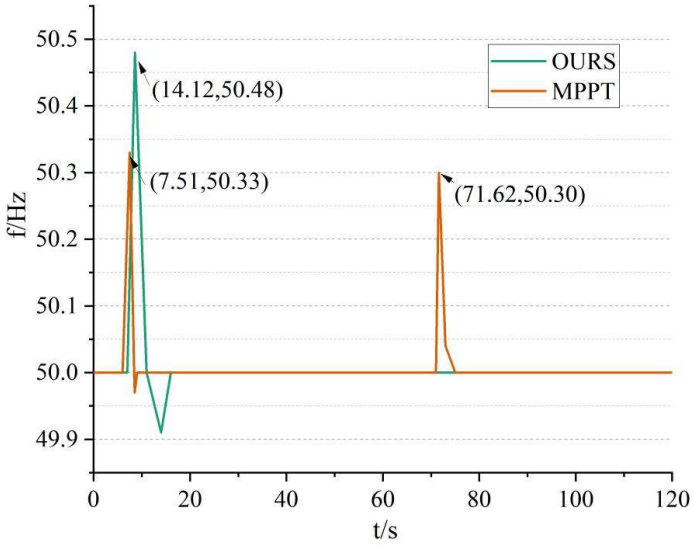

Figure 2: Frequency variation

As shown in Fig. 2 when the energy storage is at the charging threshold, the frequency overshoot under the control strategy of this paper will be larger than that of the conventional MPPT control, the frequency overshoot is 50.48 and 50.33 Hz, respectively, but under the conventional MPPT control, the system will experience the second overshoot phenomenon, and the second overshoot of the MPPT will be 50.30Hz, which will threaten the robustness of the system. In comparison, the control effect of the wind-photo-hydrogen microgrid system structure based on computational analysis proposed in this paper is superior.

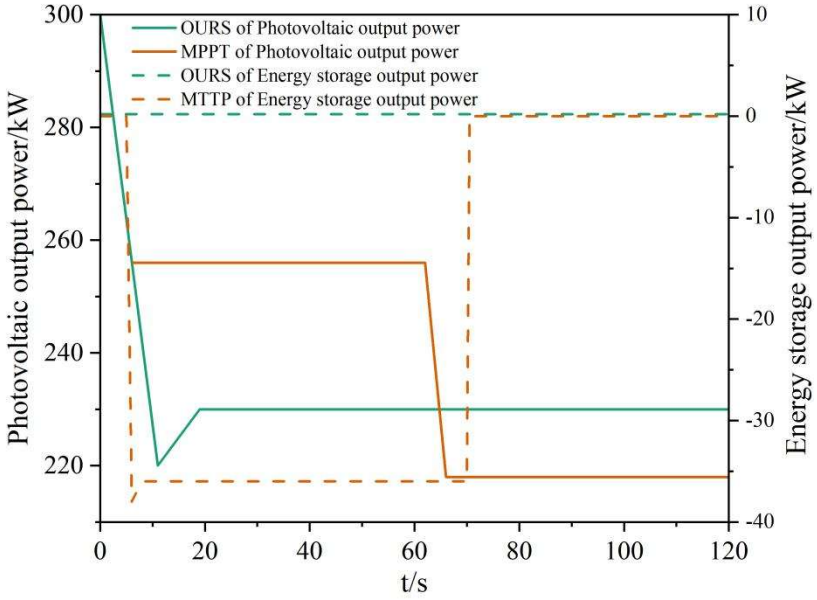

Figure 3: Variations in photovoltaic output power and energy storage output power

Analysis of the two PV output power and energy storage output power changes can be seen, using the control strategy in this paper under the PV in this case will not only take the initiative to decline its active output, PV output power in 20s after the stabilization of 230kW, to maintain the stability of the system, and compared with the conventional MPPT control of the active output decreased less, the energy storage is in the critical value of the unaffected, to maintain at 0.5kW or so, while the MPPT in the 6-70s storage output power are not stable, maintained at -36kW or so, while the MPPT in the 6-70s time. 70s the energy storage output power are unstable and maintained at about -36kW.

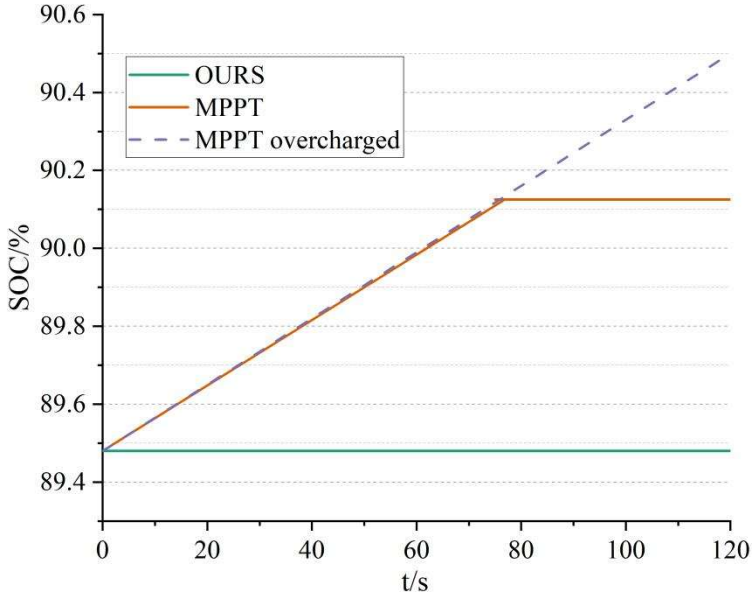

Figure 4: Changes in Energy Storage SOC

The energy storage state under conventional MPPT control exceeds the critical value of 90% and stabilizes at 90.13% after 76.9 s, which is harmful to the safety of the energy storage device. In contrast, the SOC energy storage state of the optical storage microgrid constructed in this paper based on computational analysis has been maintained at 89.45%, so the control strategy proposed in this paper can ensure the safety of energy storage operation when the energy storage is at the charging critical value.

III. B. Analysis of model predictions

After verifying the safe operation of the energy storage system under the critical state of charge (SOC), the accuracy of renewable energy output and load prediction needs to be further ensured in order to support the dynamic scheduling of microgrids and the optimal control of power allocation. In this section, based on the direct-indirect combination prediction model proposed in the previous section, we analyze the impact of prediction error on system stability through simulation experiments of photovoltaic and wind turbine output prediction, verify the applicability of the proposed prediction strategy under complex working conditions, and provide reliable data support for real-time scheduling.

III. B. 1) PV Output Forecast Results and Analysis

The output power of the PV generator set is predicted using the combined output power and load power prediction model established in this paper, as shown in Fig. 5 for the prediction results output from the combined prediction model, and compared and analyzed with the actual PV generator set output power.

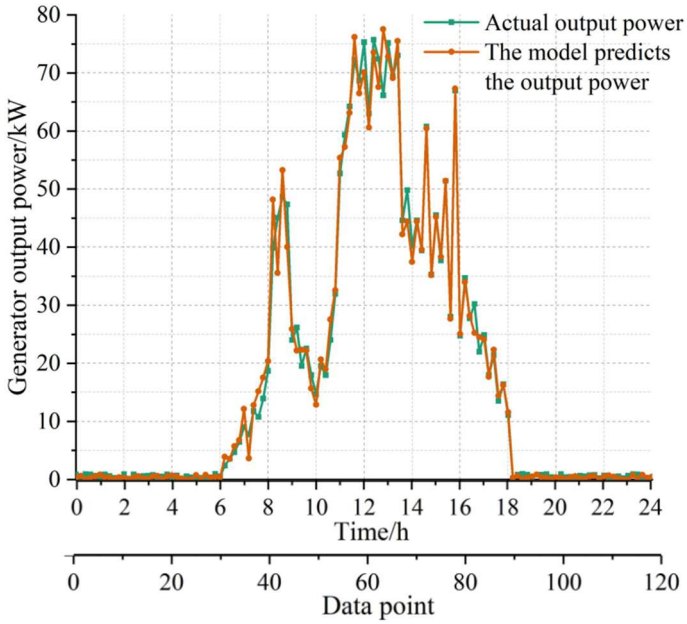

Figure 5: Model photovoltaic prediction

As shown in Fig. 5, in the first five hours of prediction, the prediction error of the combined prediction model is very small, almost completely fitting with the actual output power curve, which can realize a more accurate prediction; in the 6th to the 8th hours, there is a fluctuation of the prediction value, but in general the prediction error is small; in the 9th to the 14th hours, the light intensity is larger and the outside temperature is higher, when the PV generator set In hours 9 to 14, the light intensity is higher, the outside temperature is higher, and when the output power of the PV generator unit increases, the prediction error gradually reaches the extreme value; in hours 15 to 20, the PV output power gradually decreases until it falls to 0, and the prediction error gradually decreases. According to the prediction of 120 data points, the accuracy of the model's PV output prediction can reach 95.18%. In summary, the combined prediction model in this paper can accurately predict the output power of PV generator sets and can reduce the accumulation of errors due to the passage of time.

III. B. 2) Results and analysis of wind turbine output prediction

Using the combination prediction model established in this paper to predict the output power of wind turbines, as shown in Figure 6 for the combination prediction model output prediction results, and with the actual wind turbine power situation for comparison and analysis.

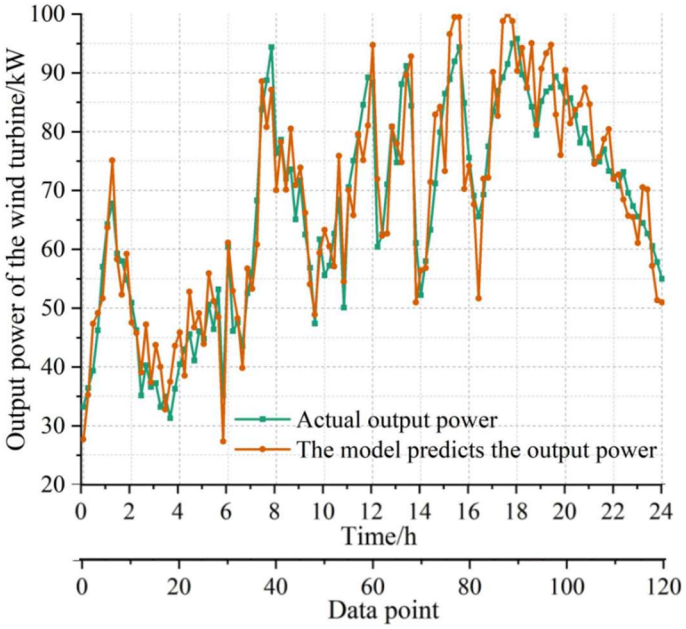

Figure 6: Combined model wind turbine prediction

In the first 7 hours of prediction, the prediction ability of the combined model is better, and the actual power curve is more suitable; in the 7th to 18th hours, the actual power value of the wind turbine is affected by the wind speed, which shows a large fluctuation, and the combined model is able to make a more accurate prediction for the sudden change of the power situation; in the 20th to 24th hours, the error is gradually reduced with the time, and the combined model is able to realize a higher prediction accuracy of the wind turbine. The combined model can achieve high prediction accuracy. According to the prediction of 120 data points, the accuracy of the model in predicting PV output reaches 80.71%. In summary, for the wind turbine power problem with strong randomness, the combined model is able to eliminate the accumulation of time errors and obtain more accurate prediction results.

III. C. Simulation analysis of microgrid operation state based on optimal allocation strategy

After verifying the accuracy of the energy storage safe operation and output prediction model, in order to further verify the engineering applicability of the microgrid optimization allocation strategy, this section analyzes the cooperative operation characteristics of the energy storage system and distributed power (DG) based on the actual operation parameters of the regional grid, and evaluates the stability of the optimization allocation strategy through the matching between the power allocation curve and the system load.

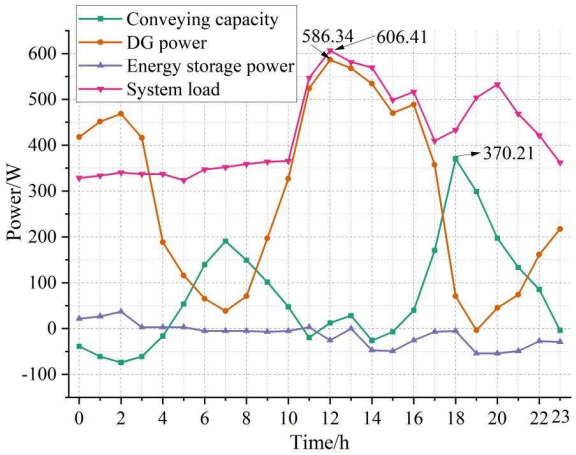

Figure 7: The operation status of the optimized microgrid

The power and minimum configured capacity of the energy storage system are 30 MW and 70 MWh, respectively. The proportion of energy storage in the regional grid is about 23.3%, and its utilization hour is 5.3 h. Through the proposed optimal configuration strategy, the output curves of the additional regulated power of the regional grid, the generation power of the DGs, the absorbed power of the energy storage, and the power of the system load are obtained as shown in Fig. 7.

As can be seen in Fig. 7, in the valley tariff, the energy storage system utilizes the low tariff for charging and then releases the energy stored in the storage at the peak load. The transmission capacity induces a peak at the moment of sunset at 18:00 with a power of 370.21 W, and the DG power peaks at 12:00 noon with a power of 585.34 W. The optimized optical storage and charging microgrid based on the computational analysis of this paper has not exceeded the system load for each power, and the highest system load is 606.41 W, which is known to be good stability.

III. D. Comparative experiment of voltage stability assessment methods based on computational analysis

In order to verify whether the methods designed in this paper, meet the needs of power system voltage stability assessment, this paper conducts an experimental analysis of the above methods. The final experimental results are presented in the form of a comparison between the assessment method based on the dimensionality reduction of the KPCA feature quantity, the assessment method based on the attention mechanism, the assessment method based on the data-driven method, and the assessment method based on the computational analysis designed in this paper.

Under the above experimental conditions, this paper randomly selects the power system voltage data from several time periods, intercepts the voltage changes of nodes A and B respectively, and conducts three experiments for each method to obtain the experimental data (a), (b) and (c). With all other conditions known, the evaluation performance of the four different methods is compared, and the experimental results are shown in Table 1. In the process of power system voltage stability assessment, “1” indicates that the voltage is in a stable state, and “0” indicates that the voltage is in an unstable state. Node A and node B are in different locations on the same line of the power system with a long interval, and the smaller the value of voltage change between them, the more stable the voltage is. At the same time, the higher the TSI and Tm, the more stable the voltage is; the larger the Pa and Gmean, the more accurate the results of voltage stability assessment.

Table 1: The performance evaluation results of four different methods

	Node voltage A/V	Node voltage B/V	Voltage variation value	TSI	Tm/%	Pa/%	Gmean/%	Evaluation result
KPCA characteristic quantity	220	215	-2.27%	0.9	90.27	92.39	91.28	1
	230	167	-27.39%	0.6	67.38	72.34	73.29	0
	240	148	-38.33%	0.5	60.33	70.18	71.02	0
Attention mechanism	230	182	-20.87%	0.8	78.29	82.36	83.20	0
	235	207	-11.91%	0.9	91.37	94.23	95.20	1
	215	137	-36.28%	0.4	41.63	69.24	70.25	0
Data-driven	240	148	-38.33%	0.6	70.06	82.35	84.01	0
	225	237	5.33%	0.9	93.74	95.27	95.24	1
	218	186	-14.68%	0.8	88.27	89.23	89.74	1
Computational analysis	230	238	3.48%	1.0	99.48	99.73	99.32	1
	240	222	-7.50%	1.0	99.95	99.22	99.83	1
	235	217	-7.66%	0.9	98.12	97.29	96.29	1

After using the power system voltage stability assessment method based on KPCA feature quantity dimensionality reduction, the voltage change values of nodes A and B are -2.27%, -27.39% and -38.33%, respectively, and the experimental data (b) and (c) are in the state of voltage instability, and the assessment results have the problem of error, which affects the safe operation of the power system.

After using the power system voltage stability assessment method based on the attention mechanism, the voltage change values of nodes A and B are 20.87%, -11.91%, and -36.38%, respectively, and the experimental data (a) and (c) are in the state of voltage instability, and the assessment results have the problem of errors, which urgently need to be further optimized.

After using the data-driven based power system voltage stability assessment method, the voltage change values of nodes A and B are 38.33%, 5.33%, -14.68%, respectively, and the experimental data (a) are in the state of voltage

instability, and there is a situation where the assessment results have errors, and there is still a need to further optimize them.

After using the data-driven power system voltage stability assessment method designed in this paper, the voltage change values of nodes A and B are 3.48%, -7.50%, and -7.66%, respectively, and the experimental data are in the state of voltage stabilization, and the assessment results do not show any errors, and the various indexes are able to meet the actual needs, and the assessment effect is better, which is in line with the purpose of this research paper.

III. E. Critical stable and unstable states

In order to further reveal the dynamic characteristics of the system under extreme operating conditions, this section analyzes the potential threat of voltage fluctuation to the system stability by comparing the difference between the energy accumulation and release processes in the critical stable and unstable states through the transient response experiments of the dc-link capacitor voltage.

In the transient response process, the voltage dynamics of the DC link capacitor is manifested in two cases: the critical steady state and the unstable state. The DC link capacitor voltage dynamics is shown in Fig. 8.

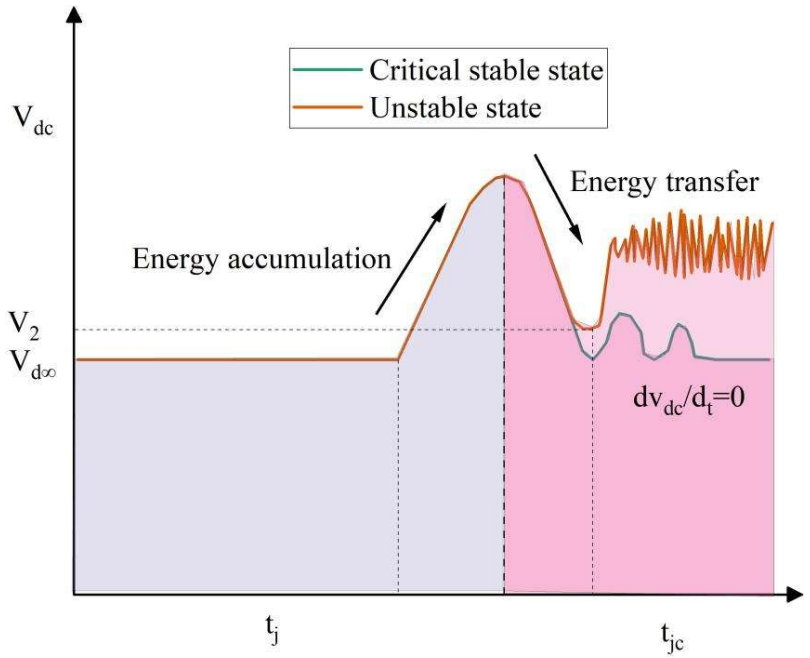

Figure 8: Dynamic capacitance voltage of DC link

In the critical steady state, the process of energy accumulation and release from the capacitor is smoother, and the system is able to return to stability more quickly, despite some fluctuations during the voltage boost. In contrast, in the unstable state, the transfer of energy is unstable and the voltage fluctuations are more violent and longer in duration. The system exhibits significant voltage spikes and the voltage continuously oscillates during the recovery process. This indicates a significant threat to the stability of the system, making it difficult for the DC link voltage to return to steady state, and the above unstable behavior usually triggers the activation of protection mechanisms to avoid further system failures.

IV. Conclusion

In this paper, a set of comprehensive analysis methods from modeling, prediction to cooperative regulation is proposed for the impact of optical storage charging microgrid output on the stability of distribution network, and its effectiveness is verified through multi-dimensional simulation experiments. The conclusions are as follows.

The direct-indirect combination prediction method significantly reduces the uncertainty of new energy output, and the prediction errors of PV and wind turbine are controlled within 4.82% and 19.29%, respectively, which provides highly reliable data support for microgrid dynamic dispatch.

The control strategy based on SOC dynamic constraints effectively avoids excessive charging and discharging, and SOC fluctuation is $\leqslant$1.55%. In the regional grid, 30MW/70MWh of the energy storage system reduces the

peak load by 6.2% (606.41W→585.34W) through the valley charging and peak discharging strategy, which verifies the economy and safety of cooperative operation.

Comparative experiments show that the evaluation method based on computational analysis outperforms the traditional method in the indexes of node voltage deviation ⩽7.66%, TSI ⩾0.9 and Gmean Gmean⩾96.29%, and the accuracy of evaluation is improved to 99.73%, which can accurately identify the critical stable and unstable states.

Funding

This work was supported by GZKJXM20240013.

References

[1] Zhang, S., Yao, L., Xue, Y., Dou, D., Yang, G., Lv, Y., & Zhang, X. (2020). Optimal operation of photothermal power station in regional power grid with high permeability of new energy. Sustainable Computing: Informatics and Systems, 27, 100388.

[2] Shi, Q., Yang, P., Tang, B., Lin, J., Yu, G., & Muyeen, S. M. (2023). Active distribution network type identification method of high proportion new energy power system based on source-load matching. International journal of electrical power & energy systems, 153, 109411.

[3] Shayeghi, H., & Alilou, M. (2021). Distributed generation and microgrids. In Hybrid Renewable Energy Systems and Microgrids (pp. 73-102). Academic Press.

[4] Espina, E., Llanos, J., Burgos-Mellado, C., Cardenas-Dobson, R., Martinez-Gomez, M., & Saez, D. (2020). Distributed control strategies for microgrids: An overview. IEEE Access, 8, 193412-193448.

[5] Lezhniuk, P., Hunko, I., Kravchuk, S., Komada, P., Gromaszek, K., Mussabekova, A., ... & Arman, A. (2017). The influence of distributed power sources on active power loss in the microgrid. Przeglad Elektrotechniczny, 93(3), 107-112.

[6] Mengelkamp, E., Gärttner, J., Rock, K., Kessler, S., Orsini, L., & Weinhardt, C. (2018). Designing microgrid energy markets: A case study: The Brooklyn Microgrid. Applied energy, 210, 870-880.

[7] Zhou, X., Guo, T., & Ma, Y. (2015, August). An overview on microgrid technology. In 2015 IEEE international conference on mechatronics and automation (ICMA) (pp. 76-81). IEEE.

[8] Bullich-Massagué, E., Díaz-González, F., Aragüés-Peñalba, M., Girbau-Llistuella, F., Olivella-Rosell, P., & Sumper, A. (2018). Microgrid clustering architectures. Applied energy, 212, 340-361.

[9] Farrokhabadi, M., Canizares, C. A., Simpson-Porco, J. W., Nasr, E., Fan, L., Mendoza-Araya, P. A., ... & Reilly, J. (2019). Microgrid stability definitions, analysis, and examples. IEEE Transactions on Power Systems, 35(1), 13-29.

[10] Alam, M. S., Al-Ismail, F. S., Salem, A., & Abido, M. A. (2020). High-level penetration of renewable energy sources into grid utility: Challenges and solutions. IEEE access, 8, 190277-190299.

[11] Medina, C., Ana, C. R. M., & González, G. (2022). Transmission grids to foster high penetration of large-scale variable renewable energy sources–A review of challenges, problems, and solutions. International Journal of Renewable Energy Research (IJRER), 12(1), 146-169.

[12] Muttaqi, K. M., Islam, M. R., & Sutanto, D. (2019). Future power distribution grids: Integration of renewable energy, energy storage, electric vehicles, superconductor, and magnetic bus. IEEE Transactions on Applied Superconductivity, 29(2), 1-5.

[13] Zhu, Z. B., Sun, S. M., Ding, Y. M., & Huang, S. P. (2023). Research on control strategy of hybrid energy storage system with optical storage microgrid. Journal of Electrical Engineering & Technology, 18(4), 2835-2845.

[14] Pang, C., Wu, H., & Jia, B. (2023). A multi-mode coordinated operation control strategy for optical storage DC microgrid. Energy Reports, 9, 230-235.

[15] Yandong, L., Yiwen, H., Nan, C., Jingyue, W. A. N. G., Xinming, S. H. A. O., Zhongchen, P. E. I., & Chuang, L. I. U. (2022). Study on power optimization method and coordinated control strategy of optical storage microgrid. Journal of Electrical Engineering, 17(1), 22-30.

[16] He, Q., Zhou, R., Li, B., & Yue, Q. (2024, June). Energy storage capacity optimization of optical storage microgrid considering customer satisfaction and depth of energy storage discharge. In Journal of Physics: Conference Series (Vol. 2782, No. 1, p. 012056). IOP Publishing.

[17] Wang, R., Wu, Z., & Sun, Z. (2024). Optimization of charging-station location and capacity determination based on optical storage, charging integration, and multi-strategy fusion. J. Green Econ. Low-Carbon Dev, 3(1), 1-14.

[18] Tianqi, L., Jing, G., Heyan, Z., & Guochen, Y. (2023). Optimization of hybrid energy storage based on micro grid optical storage and DC in certain regions. International Journal of Frontiers in Engineering Technology, 5(1).

[19] Tianqi, L., Jing, G., Fang, L., Guochen, Y., & Mingze, S. (2023). Comprehensive research on hybrid energy storage strategies of park microgrids with optical storage and DC microgrids. Academic Journal of Engineering and Technology Science, 6(1), 31-35.

[20] Zhou, H., Lu, F., & Liu, Y. (2023). Coordination control for output voltage of optical-storage independent microgrid based on adaptive optimisation. International Journal of Powertrains, 12(4), 299-310.

[21] Mlilo, N., Brown, J., & Ahfock, T. (2021). Impact of intermittent renewable energy generation penetration on the power system networks–A review. Technology and Economics of Smart Grids and Sustainable Energy, 6(1), 25.

[22] Chang, W. N., Chang, C. M., & Yen, S. K. (2018). Improvements in bidirectional power-flow balancing and electric power quality of a microgrid with unbalanced distributed generators and loads by using shunt compensators. Energies, 11(12), 3305.

[23] Elsamahy, M. (2022). Reducing Microgrids Integration Complexity in Distribution Networks Considering Bidirectional Power Flow in SFCLs. IEEE Access, 10, 80365-80378.

[24] Weigert, G. R., Gurski, E., & Benedito, R. A. D. S. (2019). Computational algorithm for stability analysis of distribution networks with distributed generation. Brazilian Archives of Biology and Technology, 62, e19190010.

[25] Rizvi, S. M. H., & Srivastava, A. K. (2023). Integrated T&D voltage stability assessment considering impact of DERs and distribution network topology. IEEE Access, 11, 14702-14714.